INTERNATIONAL ATOMIC ENERGY AGENCY
UNITED NATIONS EDUCATIONAL, SCIENTIFIC AND CULTURAL ORGANIZATION

INTERNATIONAL CENTRE FOR THEORETICAL PHYSICS
34100 TRIESTE (ITALY) - P.O.B. 586 - MIRAMARE - STRADA COSTIERA 11 - TELEPHONE: 2240-1
CABLE: CENTRATOM - TELEX 460392-1

SMR/390 - 14

WORKING PARTY ON "FRACTURE PHYSICS"
(29 May - 16 June 1989)

FUNDAMENTALS OF SILICON FRACTURE

G. MICHOT
Ecole Nationale Superieure Des Mines de Nancy
Laboratoire de Physique Du Solide
Parc de Saurupt
Nancy 54042
France

Crystal Properties and Preparation. Janv.89 - Trans. Tech. Publ.

FUNDAMENTALS OF SILICON FRACTURE

G. MICHOT

Laboratoire de Physique du Solide associé au CNRS (URA D0155)
Ecole des Mines - Institut National Polytechnique de Lorraine
Parc de Saurupt - 54042 NANCY Cedex (France)

Laboratoire pour l'Utilisation du Rayonnement Electromagnetique
91405 ORSAY Cedex (France)

In memory of S.M. OHR

ABSTRACT

Critical stress for brittle cleavage of Silicon at 20°C along {110} planes was determined, then compared to previous results on {111} planes. The plastic zone developped at high temperature around the crack tip was characterized by X-Ray Topography and etch pit counting (glide plane, Burgers vectors, dislocations distribution). The influence of the load level on the plastic zone growth was emphasized. The toughness increase due to plastic relaxation was also investigated either under creep conditions or under dynamic loadings.

INTRODUCTION

- Mechanical properties of semiconductors have often been neglected in the past, merely because of their limited influence in Silicon device applications.

Furthermore the few difficulties encountered in VLSI technology like chip cutting have been bypassed by sawing in place of scribing and cleaving. However brittle fracture is still a major source of solar cell rejection. Thus a better understanding of the cleavage process is required either to avoid fracture or to control it (like in laser diodes manufacture for instance). Dislocation content is well controlled in Silicon technology, it is not possible yet for III-V compounds. In this latter case a decay of optoelectronic properties is related to an increase of dislocation density. Therefore control of dislocation nucleation and development during crystal growth or during service, is a major priority in microoptoelectronic technology. In particular stress risers can improve dislocation emission even under low level loadings : microcracks for instance, easily introduced during processing can act as dislocation sources. The sudy of crack-dislocation interaction is of general importance, thus of practical interest for structural materials (steels, aluminium alloys, etc), far beyond the limited scope of Silicon.

- However Silicon has several advantages which give the best conditions for such basic studies.

1) Silicon single crystals of high quality (zero grown-in dislocations, a very few defect amount) and large size are available.

2) A totally brittle, limited, cristallographic cleavage can be introduced in the material at room temperature. The failure of the material is readily explained by the strong lattice friction that opposes dislocation motion, because of covalent bonding.

3) At sufficiently high temperature dislocations have gained by thermal activation a sufficient mobility to glide and multiply. Because of an exponential variation with temperature, Silicon allows one to cover the entire range from totally brittle to fully plastic behaviour. At ≈ 1000 K the plasticity is low enough to follow experimentally the growth kinetics of plastic zone with reasonable time intervals. Under 800 K material plasticity almost reduces to zero : in these conditions quenching from higher temperature will freeze-in the dislocation pattern.

4) Dislocation mobility has been extensively studied as a function of stress, temperature and doping.

5) X-Ray topography is a diffraction imaging technique very well suited to the study of non absorbing single crystals like silicon. Limit of spatial resolution of XRT lies in the μm range and is poor compared to that of transmission electron microscopy, but a strong compensation is the possibility of the method to check non destructively the defect content in the bulk of samples thick enough to be safely handled an submitted to well defined stress conditions. In fracture studies XRT can help greatly in establishing not only "static" feature (for instance identification of activated slip systems), but also "dynamic" ones such as the threshold value of the stress intensity factor for dislocation emission, growth kinetics of the plastic zone, estimates of the effective stress, etc. The field of possible applications of XRT has been considerably extended by the use of the intense and tunable synchrotron radiation which dramatically reduces to some seconds the exposure time. XRT has been sucessfully applied to characterization of cleavage crack geometry, shape and dislocation content of plastic zones developped in both creep or dynamic conditions.

In the following the main results are summarized and critical problems discussed. The paper will be divided into two parts, the first one devoted to the brittle behaviour of Silicon, the second one to the crack-dislocation interactions.

PART A - BRITTLE FRACTURE

I - EXPERIMENTAL TECHNIQUES

- Double cantilever beam testpieces were cut from {112} and {100} wafers (figure 1) grown by Wacker ("waso" quality). Both floating zone (FZ) and Czochralski (CZ) single crystals have been used for this study ; differences in growth conditions lead to differences in microdefects content, but no effect of Silicon origin has been detected on the brittle behaviour of the material.

- Machining is achieved by sparkcutting and/or abrasion. After mechanical then chemical polishing the sample thickness B ranges between 450 and 800 micrometers. The samples are pre-cracked at room temperature by forcing an alumina wedge into the notch [1,2]. The cracked sample is then clamped in a tensile stage by introducing two rods into the pin holes, then the crack is loaded at 20°C under mode I opening [5] until propagation occurs : this crack advance can be achieved up to six times before complete breaking of the sample.

Topographs are recorded on Ilford L4 100 μm nuclear emulsion plates.

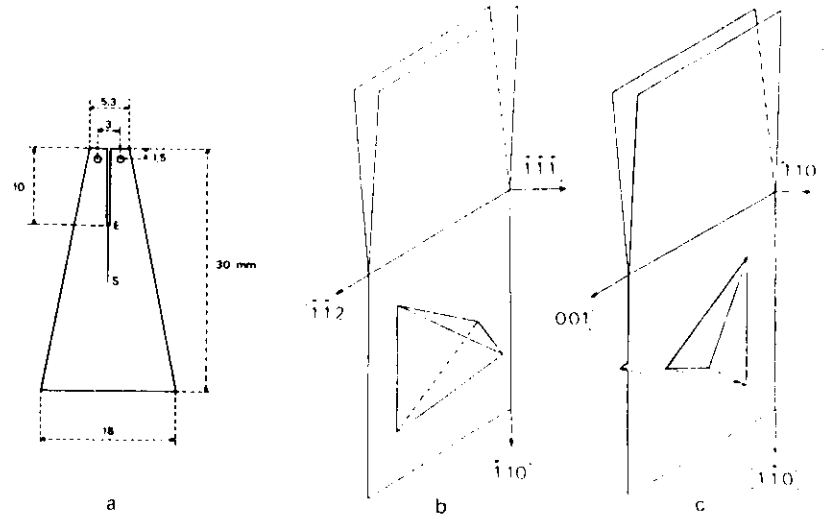

Figure 1 - a) Sample shape : W = 30 mm, the crack length a is equal to the notch depth, 8.5 mm, plus ES. The sample thickness is B.
b) Alpha orientation *c) Gamma orientation*

II - CRACK CHARACTERISTICS

- The crack features, i.e. length, plane misorientation versus the ideal crystallographic plane [2,3], crack tip orientation [2], are determined by XRT [4] using the Lang Method. A satisfying measurement of the misorientation angle was obtained : the deviation is less than 4° from a {111} plane in the alpha orientation (figure 1b) and generally less than 5° from a {110} plan in the gamma orientation (figure 1c). These values are geometrically deduced from measurements of the crack image width as recorded on X-Ray topographs. Crack lengths measurements on topographs are much more accurate than optical ones, ranging from 2 to 10 millimeters.

- In X-Ray topography the poor resolution is counterbalanced by a high sensitivity to lattice strains : very small defects on the crack surface give rise to strong contrasts (figure 2), the crack quality can therefore be easily checked. For instance closure imperfection is revealed by figure 3 which displays a moire pattern typical of a mismatch between the two crack surfaces after unloading (the crack tip belonging to both surfaces it is a roration Moire corresponding to a slight mode III opening).

Figure 2 - X-Ray Topograph $\vec{g} = 31\bar{1}$.
β orientation
Accidents are clearly visible on crack surface

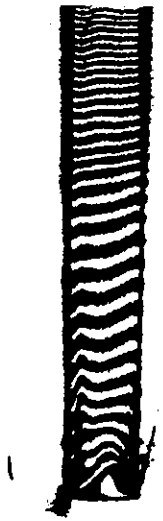

Figure 3 - Topograph $\vec{g} = 111$
γ orientation
The Moire pattern is modulated by Pendellösung fringes

III - SILICON TOUGHNESS

III.1 - Basic background

- In the coordinate system of figure 4, the elastic stress field around a sharp crack under mode I loading is expressed by the relation :

$$\sigma_{ij} = \frac{K_I}{\sqrt{2\pi r}} g_{ij}(\varphi) \qquad (1)$$

where $g_{ij}(\varphi)$ are known functions of phi [5]. The so-called stress intensity factor K_I depends on the external loading through a calibration function f(a/w) :

$$K_I = P\, f(a/w) / B \qquad (2)$$

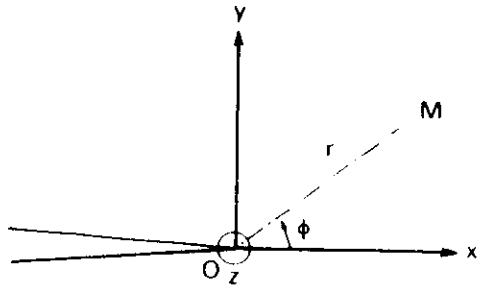

Figure 4

Cartesian coordinate system : y is perpendicular to the crack plane, z is parallel to the crack tip. r and φ are polar coordinates.

For our tappered DCB samples this function only increases slightly with crack length [6]. During loading propagation occurs for a critical load P_c, i.e. when K_I reaches a critical value K_{Ic} which is assumed to be a physical characteristic of the material, called toughness.

- The energetics approach developed by Griffith [7] assumes that crack growth occurs if the energy required to increase the crack length of da can just be delivered by the system. Because crack velocity in brittle materials is

use to the sound velocity the external work can be neglected during opagation and only part of the elastic stored energy U is released to create o new surfaces :

$$G_c = -\frac{1}{B}\left(\frac{dU}{da}\right)_\delta = 2\gamma \qquad (3)$$

is called critical energy release rate or crack extension force, γ is the rface energy for fracture (probably different from thermodynamic surface ergy). Because the load-displacement curve is linear in the elastic range igure 5) another expression can be derived, introducing the sample compliance = δ/P (δ is the crack opening) :

$$G_c = \frac{P_c^2}{2B}\left(\frac{\partial C}{\partial a}\right)_\delta \qquad (4)$$

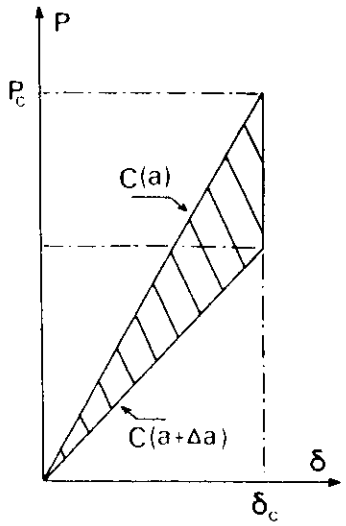

Figure 5

Compliance variation with crack advance. The dashed surface corresponds to energy required for creation of two new surfaces, i.e. $\gamma B \Delta a$

- It has been shown [8,9] that the physical quantities K_{Ic} and γ obtained two different methods are not independent :

$$2\gamma = K_{Ic}^2\left(\frac{1-\nu^2}{E}\right) \qquad (5)$$

A plane strain condition is assumed, E is the Young's Modulus and ν the oisson ratio).

III.2 - Easy cleavage plane

As far as single crystals are concerned, cleavage can occur on several planes. According to Orowan [10] and Gilman [11], the theoretical cleavage stress and the surface energy for {hkl} planes are proportionnal to the ratio of the Young's Modulus E versus the interplane spacing d_{hkl}. In covalent materials the lower ratio corresponds to {111} planes. However, III-V compounds fail along {110} planes [12]. This discrepancy is probably specific to the partial ionicity of the bonding in these materials : {111} planes have a polar character due to the stacking sequence (one layer of element III, one layer of element V... (figure 12), conversely {110} planes are neutral, no additionnal electrostatic energy is required for bond breaking.

- If {110} cleavages are observed on neutral {110} planes in III-V compounds we may assume that it is also possible on, obviously neutral, {110} planes in Silicon. Actually, some {110} crack observations have been reported in the literature [13-16] ; the authors observe that this cleavage generally deviate from the ideal {110} plane. However it has been shown [3,17,18] that under given conditions, such a crack can be introduced and propagated in Silicon.

III.3 - Results

- Using the critical load method, the K_{Ic} is related to P_c through the calibration relation (equation 2). The obtained values for {111} cleavages, as measured by S^t John [1] and Michot [19], using the same techique are very closed, 0.96 and 0.93 MPa$\sqrt{m}$ respectively . The measured value for {110} cleavage [18] is not very different :

$$K_{Ic}^{110} = 0.89 \pm 0.04 \text{ MPa}\sqrt{m}$$

- By the energetics method, measured surface energy are equal to 2.87 J/m^2 for {111} planes [1] and 2.45 $\pm$ 0.40 J/m^2 for {110} planes [18].

III.4 - Discussion

- We are confident about our experimental result on {110} cleavages because they verify the theoretical relation (equation 5) within the experimental scatter. We have choosen results obtained by the critical load approach because of the low scatter :

$$\gamma_{110} = 2.25 \text{ J/m}^2 \qquad [18]$$

$$\gamma_{111} = 2.70 \text{ J/m}^2 \qquad [1]$$

- A rough approximation based either on the Gilman model [11] or on the planar bond density [17,18] gives a theoretical ratio $\gamma_{111}/\gamma_{110}$ equal to 0.68 and 0.82 respectively . Our experimental ratio is strikingly larger than unity. Because optical micrographs and X-Ray topographs [3,18] indicate that {110} cleavages are cleaner than {111} ones and comparable to those obtained in III-V compounds, we assume that our γ_{110} value is close to the true value, and that all the surface defects (ledges, tear marks, rivers... [20]) observed on {111}

cleavages have required some additionnal energy consumption [21,22,28]. In these conditions, using the Gilman ratio, i.e., 0.68, the expected γ_{111} value equals 1.5 J/m^2. This value compares quite well with other data presented in the literature [13,23], 1.14 J/m^2 and 1.23 J/m^2 respectively , with some theoretical predictions [24,25], 1,41 J/m^2, but drastically differs from Gilman evaluation [11], 0.82 J/m^2.

- Our γ_{110} value (2.25 J/m^2) also compares fairly well with other data [13,17], respectively 1.90 and 1.81 J/m^2. However is seems that the cleavage technique is too sensitive to crack surface quality and to any parasitical energy dissipation source : for instance, some energy is wasted by sound waves during crack propagation (figure 6). But one should be aware that theoretical calculations are also very sensitive to the choice of interatomic potentials.

Figure 6

Optical micrograph of the cleavage crack. Reflection of the sound waves on the sample boundary (crack propagates from left to right)

III.5 - Crystallographic anisotropy

- Experimentally, crack nucleation is enhanced by scratching the root notch with a wolfram blade. This heavy damage leads to a crack spreading on different planes, giving rive to a misorientation δ of the cleavage surface versus the ideal one (Section II).

- For $\{111\}$ cleavages, the crack front propagates towards $[1\bar{1}0]$ direction, probably on (111) terraces connected by $(11\bar{1})$ ledges as schematized (figure 8). Some roughness can thus be detected, characterized by faint lines parallel to <110> directions (figure 7). These patterns, typical of anisotropic behaviour of material, indicate the preferential propagation directions. Macroscopically, when the propagation direction $[1\bar{1}0]$ is not parallel to the sample surface (figure 9), crack propagation from OS to O'S' leads to a departure η of the crack plane ; in order to minimize the corresponding energy increase, the crack is likely to re-start on a new set of $\{111\}$ planes. This change of propagation direction gives rise to a pronounced surface accident, which was often observed.

- Perfect $\{110\}$ cleavages (line GH of figure 10) are equivalent to a mixture of two sets of $\{111\}$ cleavage planes on the atomic scale (broken line G'H'). Non ideal $\{110\}$ cleavage should therefore behave like $\{111\}$ cleavages.

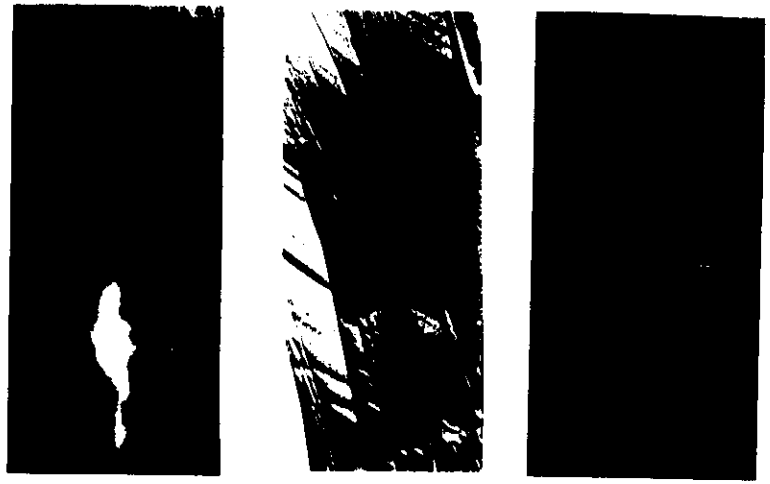

Figure 7 - Observed faint lines (arrows) are parallel to <110> directions. These micrographs correspond to two different orientations, (called alpha and beta (figures 10 and 11 of part B)).

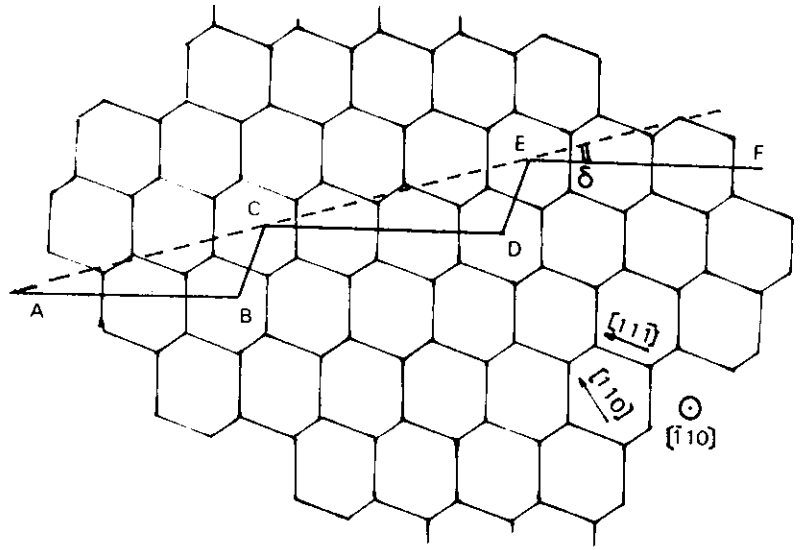

Figure 8 - $(1\bar{1}0)$ section of a covalent crystal. Only the longest bonds belong to the page plane.

i.e. propagate in <110> direction common to the two sets of planes. However there is a fundamental difference in behaviour, there is only one possible propagation direction <110> per {110} plane. When this direction is parallel to the sample surface (orientation γ, figure 11), propagation is straightforward, the misorientation δ is kept constant and the surface quality is enhanced, the previously mentionned disruptive mechanisms being avoided. Conversely if this direction is no longer parallel, the deviation η (figure 9) is always increasing : experimentally for this configuration we generally observe a very short {110} crack who deviates on transverse {111} planes until complete fracture of the specimen.

- Comment : the best {110} cleavages have been obtained in III-V compounds as emphasized before. This could indicate that the energy contribution to ledge formation is much higher in III-V compounds. This is not surprising because these ledges correspond to polar planes in these structures (figure 12).

III.6 - Microscopical mechanisms

The idea that propagation of non ideal crack takes place on two sets of {111} planes leading to a <110> propagation direction , probably still holds for a perfect crack. This assumption is based on the experience accumulated on dislocation behaviour in covalent materials [26] : stability of either dislocation or crack tip is maximum along the dense <110> direction of the lattice because of the highest number of bonds to be broken. By analogy crack should advance by nucleation and lateral spreading of kinks [27] (figure 13a,b). As mentionned before we have not been really successfull in propagating such a crack with the tip parallel to <110> so far. Conversely the easy propagation observed for gamma orientation could be also related to the fact that : i) the crack tip is a low density direction of the lattice, ii) no kink nucleation is required (figure 13c).

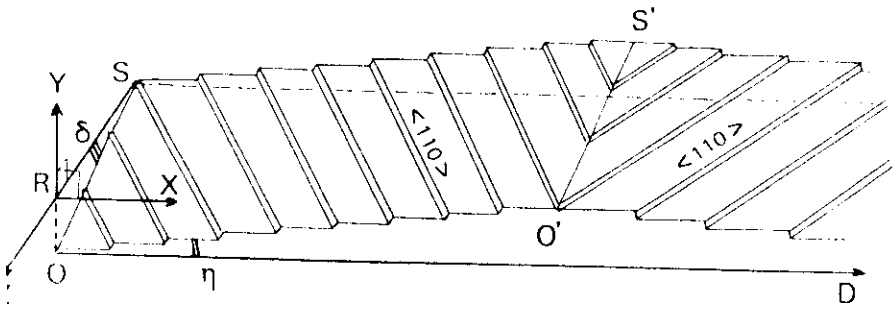

Figure 9 - OS is the crack tip. RS is the sample width (B). OD is the macroscopic propagation direction. ZRX is the ideal cleavage plane.

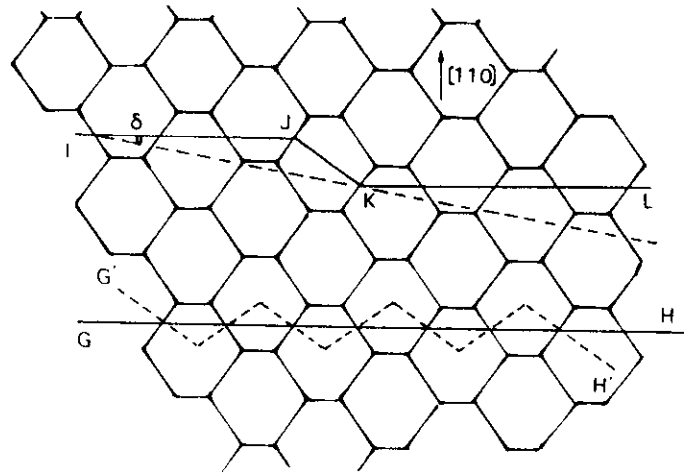

Figure 10 - Atomic crack paths for {110} cleavages (perfect cleavage GH or G'H', misoriented cleavage IL)

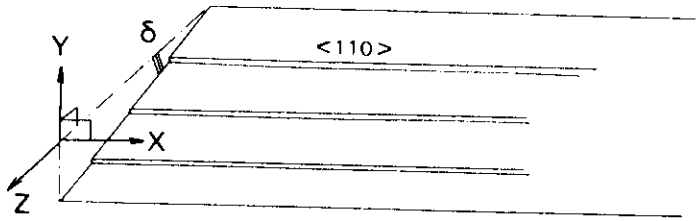

Figure 11 - Easy propagation of a slightly misoriented {110} cleavage.

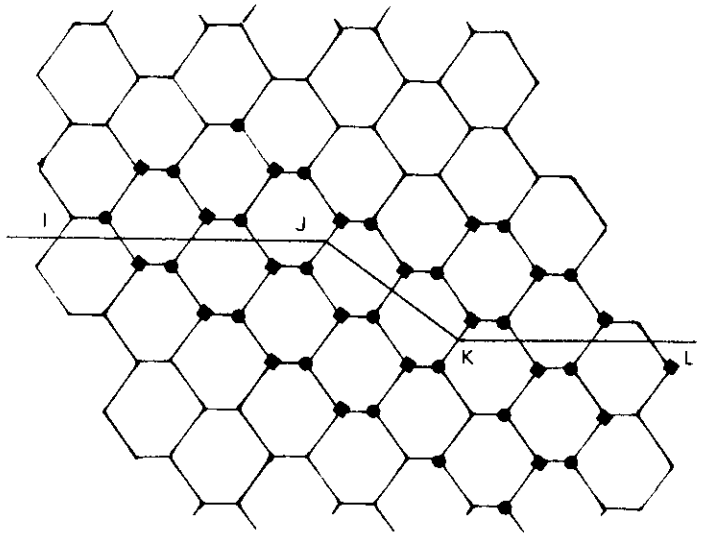

Figure 12 - Theoretical {110} cleavage with a ledge, in III-V compounds (III and V elements are represented by different symbols).

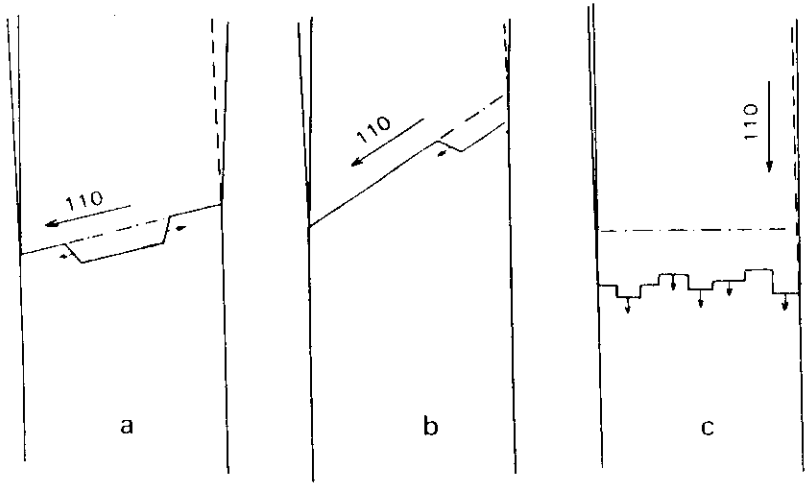

Figure 13 - a) The crack tip advances by nucleation and spreading of a double kink.
b) Nucleation takes places at the most stressed point, only one kink has to be nucleated.
c) For γ orientation no nucleation is required ; crack tip shape is probably controlled by some "line tension" as for dislocations.

PART B - PLASTIC BEHAVIOUR

The stress concentrations that arise at a crack tip induce a plastic deformation in the neighbouring material during high temperature loading. This plastically strained region is known to modify the conditions for further crack propagation. In spite of the importance of crack relaxation by dislocations in fracture problems, amongst all the related studies no experiments have been performed allowing a complete microstructural and mechanical study. Very accurate in situ characterization of plastic zones can be achieved by T.E.M. [29-38] but there is no way to correlate these observations with the poorly controlled external loading. An other point is that thin foils are not likely to behave like bulk material, especially in brittle solids : the probability to encounter a bulk dislocation source is negligible, most of the dislocations are emitted from the crack tip itself, but probably under stress level never sustained in bulk material [39]. Etch pit studies performed either on DCB samples [40-43], or on four point bending samples [40,45] help to characterize such mechanical tests but the link between the material strengthening and the dislocation characteristics is difficult to establish. Finally, eventhough XRT methods are useless for observation of the relaxation mechanisms very close to the crack tip, they allow a partial characterization of the plastic zone in a bulk sample under well defined loading conditions [1,2,4,46-48].

The ultimate aim of this study is to foresee the toughness increase of the material as a function of the external parameters which control plastic zone growth (time, temperature and loading). Initially we were interested in solving the simplest situation, i.e. by applying a constant load (creep conditions) : after a transitional period, which can be followed by in situ XRT, the equilibrium configuration has to be achieved. Characterization of such equilibrium plastic zone (glide plane, Burgers vector, dislocation density) has been performed by XRT and etch pits methods. Then we have tried to figure out the interaction mechanisms between cracks and dislocations through our experimental results. Finally an oversimplified equlibrium model of the plastic zone has been developed in order to tackle more complicated loading regimes, like constant loading rates or constant opening rate, which loading situations allow a study of the brittle to ductile transition behaviour of the material.

I - EXPERIMENTAL

- Two sets of experiments have been performed with either the conventional devices available at the laboratory (tensile machine, X-Ray generator) or using the Synchrotron facilities of L.U.R.E. (Laboratoire CNRS - Université de Paris Sud - Orsay, France).

- At the laboratory a high temperature stage has been built [18] and fitted to an 1185 Instron tensile machine. Either the opening rate $\dot{\delta}$ of the crack or the load P/loading rate $\dot{P}$ can be imposed. Thermal treatment temperature has an accuracy of 0.3°, and can be raised up to 1000°C. Forming gas (10 % H_2, 90 % N_2) was preferred to vacuum. Conventional XRT was performed either with a 20 kW generator (silver rotating anode) or with a 1,5 kW generator (molybdenum anode). The exposure time ranges from one to two hours. Conventional XRT has been used only to characterize the dislocation pattern after cooling of the sample.

- For in-situ experiments two different devices have been used. For creep experiments the load is applied directly by a system of wires and pulleys an transmitted to the moving grip through metallic bellows as described in detail in reference [49]. For dynamic experiments, the signal delivered by a wave form generator is transformed into a force by an electromagnet whose airgap is kept constant by a feedback control [50]. Topographs were taken on a two crystal spectrometer with the so-called (+,+) setting. The X-Ray beam was first reflected on a Ge crystal and then diffracted by the sample, set at a 220 Bragg reflection, with a selected wavelength of 0.08 nm. Topographs were recorded on L4 50 µm nuclear emulsion plates. The exposure time is typically 30 s when the DCI storage ring ran at 1,72 Gev, 200 mA. The sample-to-plate distance is about 3 cm which ensures for images of fixed dislocations a geometrical resolution comparable to that of the conventional Lang technique (at least at 20°C).

- Sirtl etchant has been used to reveal the intersections of dislocations on both cleavage surface and lateral faces of the sample. From etch pit counting the dislocation distribution in the plastic zone can been determined.

II - GROWTH KINETICS OF FZ SILICON UNDER CREEP CONDITION

II.1 - Results

This paragraph summarizes the results obtained at different temperatures under different load levels [51]. First of all, no plasticity has been detected for K_I values smaller than a threshold value K_I^{min} = 0.25 MPa$\sqrt{m}$ [12] (the value is nearly independant of temperature in the range 700-800°C). Above this value dislocation generation occurs. The series of topographs of figure 1 shows the outbreak and development of dislocations at different intervals of time after loading at t = 0 (T = 700°C, K_I = 0.66 MPa$\sqrt{m}$). For alpha orientation the plastic zone consists of five lobes. The plastic zone size, d, is defined by the distance between the leading dislocation (first emitted dislocation) and the crack tip, averaged on the four fully developed lobes. Figure 2 plots the evolution of d versus time at different temperatures for a given K_I value : for high loading times the plastic zone sizes tend towards a common value. Figure 3 plots the evolution of d versus time under different loads for a given temperature : after a first stage of rapid growth (stage I), whose rate is increasing with K_I and T, the plastic zone saturates (stage II) ; the limiting size strongly depends on K_I value but not on temperature.

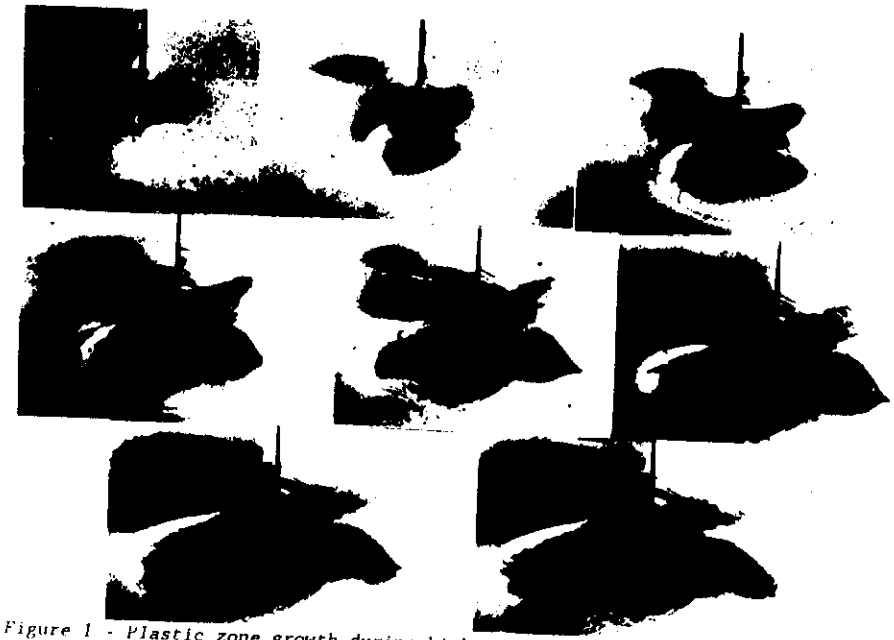

Figure 1 - Plastic zone growth during high temperature loading (T = 700°C, K_I = 0.66 MPa$\sqrt{m}$, t = 0, 10, 20, 30, 45, 60, 90 and 120 minutes)

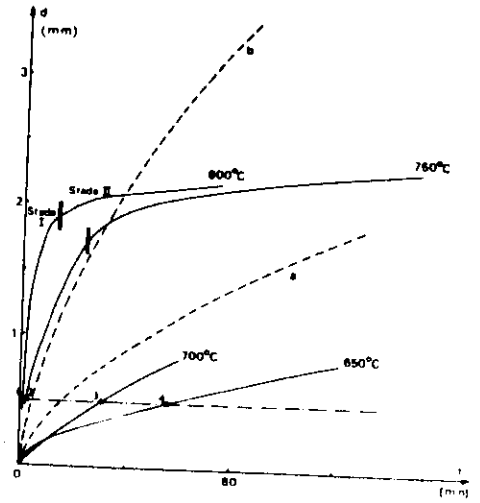

Figure 2 - Evolution of the plastic zone size versus time for different temperatures (K_I = 0.66 MPa$\sqrt{m}$)

II.2.2 - Saturation regime

- The small slopes $\dot{d}(t)$ measured in stage II leads to effective stress levels below 2 MPa. This value is smaller than the expected contribution of the singular applied stress field τ_s. However the contribution of the dislocations of the fully developed plastic zone to the internal stress field τ_i is not likely to be negligible, thus an estimate of this contribution has been done, based on etch pit counts.

- From micrographs observations, as shown figure 4, the dislocation distribution n(d) has been determined. The results obtained at 750°C under different loading levels are summarized figure 5a. The corresponding samples have been loaded two hours, thus we may consider that these results are representative of dislocation configurations in stage II. An inverse pile-up is observed. By distributing dislocations on a square net a rough estimate of the internal stress field ahead of the pile-up has been made [53], values obtained on nine samples range from 3 to 13 MPa. So in order to fulfill the equilibrium equation we conclude that the elastic stress field must be negative at large distances from the crack tip. The vanishing, but positive, singular stress field τ_s cannot obviously account for this result, a negative non singular term has to be introduced in the stress field expression :

$$\tau = \frac{K}{\sqrt{2\pi r}}\, g(\varphi) - |C(\varphi)|\sqrt{r} + \ldots \qquad (3)$$

This term comes from the sign inversion of the shear stress on neutral fibers resulting from the bending of the sample arms, as shown in figure 6, this contribution must be negative. It increases with r, leading to a confinment of the plastic zone. This is an example of the limitations of small scale yielding theory [54] which assumes that plastic zone size depends only on the K_I value.

- For a plastic zone of N dislocations, the numerical calculation of the internal stress field roughly follows a square root variation :

$$\tau_i \propto N^{1/2} \qquad (4)$$

In the mean time the variation of N with K_I follows (figure 5b) :

$$N \propto K_I^{8}$$

This means that τ_i varies as K_I to the fourth while $|C(\varphi)|$ is probably proportional to the load, i.e. to K_I. This result explains the high sensitivity of the plastic zone size with K_I (figure 3).

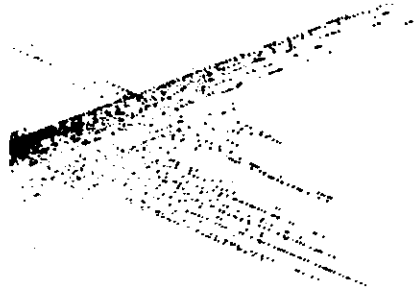

Figure 4 - Etch pit observations on a half-sample (alpha orientation)

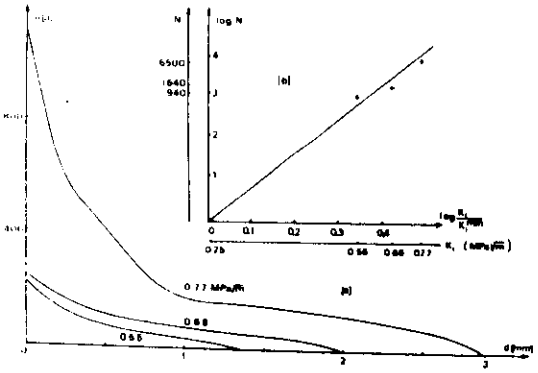

Figure 5 - a) Dislocation distribution n(d) after two hours at 750°C under different K_I values. n(d) is the number of etch pits counted between d and (d + 0.1 mm).
b) Corresponding integrated number of dislocations versus K_I values

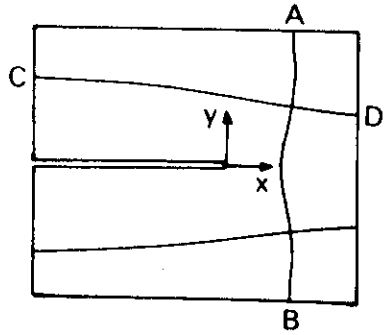

Figure 6 - Position of the neutral fiber for σ_{yy} (line AB) and σ_{xx} (line CD) components of the stress field as determined by finite element method [53]

II.3 - Conclusions

Round about one micrometer from the crack tip where the singularity of the elastic stress field is dominant, dislocations are emitted and pushed away from the crack tip. The dislocation density increasing, the internal stress acting on the leading dislocation increases too and overcomes the singular stress at a distance of several hundred micrometers. Plastic zone growth is then controlled by this internal stress field (stage I). For extensions in the order of a millimeter, the increasing non singular part of the elastic stress field opposes the internal stress field, thus lowering the plastic growth rate (stage II), tending to an equilibrium configuration. Because of the very small slope measured in stage II, relaxation is probably not complete. This means that some dislocation rearrangements are still possible, as long as the dislocation backstresses are not high enough to stop the dislocation source activity. However we considered afterwards that relaxation was nearly complete.

III - DISLOCATION CONFIGURATIONS

III.1 - Characterization method

As previously mentionned, saturation of plastic zone is assumed. Three different cristallographic orientations have been studied (figure 10 to 12). Alpha and beta orientations are relative to $\{111\}$ cleavage cracks whereas gamma orientation is relative to $\{110\}$ cleavage cracks. For any orientations dislocations will develop in those $\{111\}$ planes that cut the crack tip [2,19] (figure 7).

The slip systems have been characterized by XRT in plastic zone regions of low enough dislocation density in order to consider either the individual dislocation or a limited set of dislocations. The Burgers vector is determined through the extinction criterion $\vec{g}.\vec{b} = 0$, where $\vec{g}$ is the diffraction vector. This rule is difficult to check when the active slip plane is observed under a grazing incidence (planes $(\bar{1}\bar{1}1)$ of figure 8 for instance) but quite easy when the reflected beam direction $\vec{R}$ is close to some <111> direction (plane (111) of figure 8). Generally 111 and 220 diffraction vector have been choosen but when in doubt, 311 and 400 reflections have been used. Figure 9 displays some examples of blurred contrasts, characteristic of extinction conditions.

II.2 - Results

Slip systems in covalent crystals can be conveniently represented by the Thomson tetrahedron (figures 10 to 12).

III.2.1 - Alpha orientation (figure 10)

As expected for mode I loading no dislocations are observed in the crack plane (111) because of the lack of shear stress acting on this plane. $(\bar{1}11)$ planes display a low number of dislocations with either $a/2[\bar{1}0\bar{1}]$ or $a/2\ [0\bar{1}\bar{1}]$ Burgers vector (a is the silicon parameter). Thus, as a rough estimate, dislocations divide up into 50 % of dislocations with $\vec{b}$ parallel to the crack plane (slip systems $(1\bar{1}\bar{1})[0\bar{1}1]$ and $(\bar{1}1\bar{1})[\bar{1}01]$) and 50 % of dislocations on slip systems $(11\bar{1})[\bar{1}01]$ and $(\bar{1}11)[0\bar{1}\bar{1}]$. Dislocations with $\vec{b}$ belonging to both $(1\bar{1}\bar{1})$ and (111) planes, i.e. $a/2\ [\bar{1}\bar{1}0]$ are in the minority.

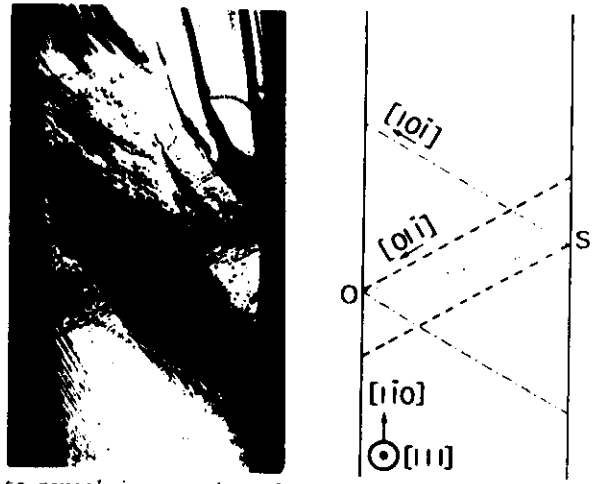

Figure 7 - a) Etch pits revealed on crack surface after complete fracture of the sample
b) Corresponding cristallographic orientation (alpha orientation, see figure 10). OS is the crack tip

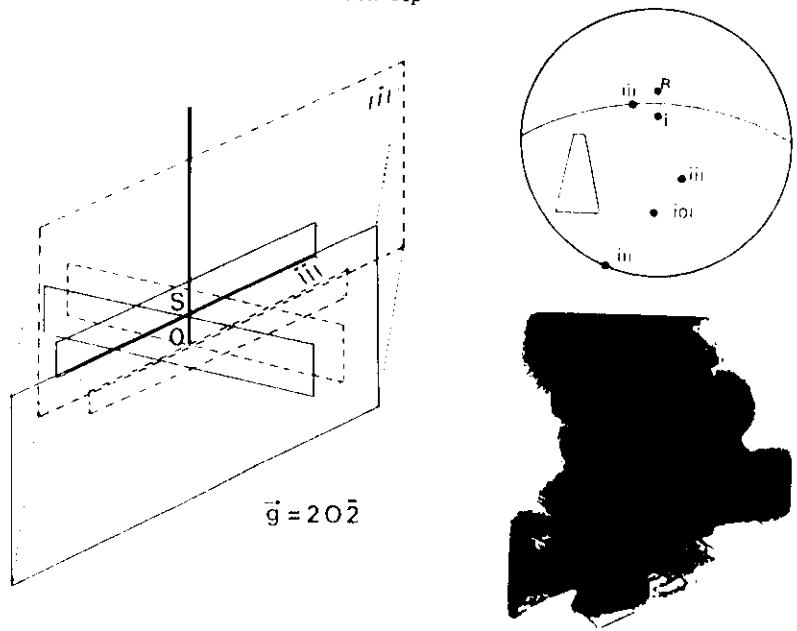

Figure 8 - a) Projection of the plastic zone volume parallelly to the diffracted beam $\vec{R}$ as recorded on topographs - Beta orientation, $\vec{g} = 20\bar{2}$
b) Crystallographic orientation
c) Corresponding topograph

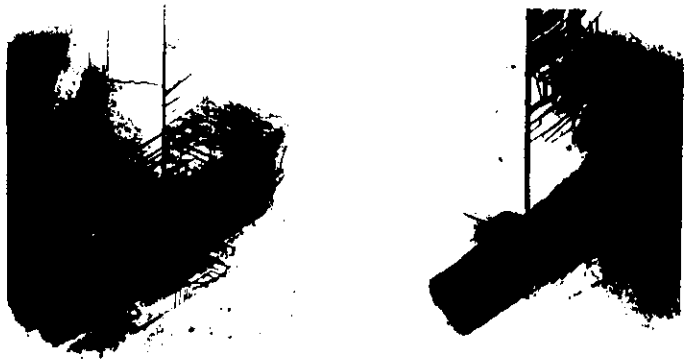

a) $\vec{g} = 1\bar{1}\bar{1}$ b) $-\vec{g} = \bar{1}1\bar{1}$

Figure 9 - The slip system $(1\bar{1}1)[\bar{1}01]$ (upper right part of (a)) is out of contrast in (b). At the opposite, $(1\bar{1}\bar{1})[110]$ (upper left part of (b) is out of contrast in (a) and visible in (b) (beta orientation)

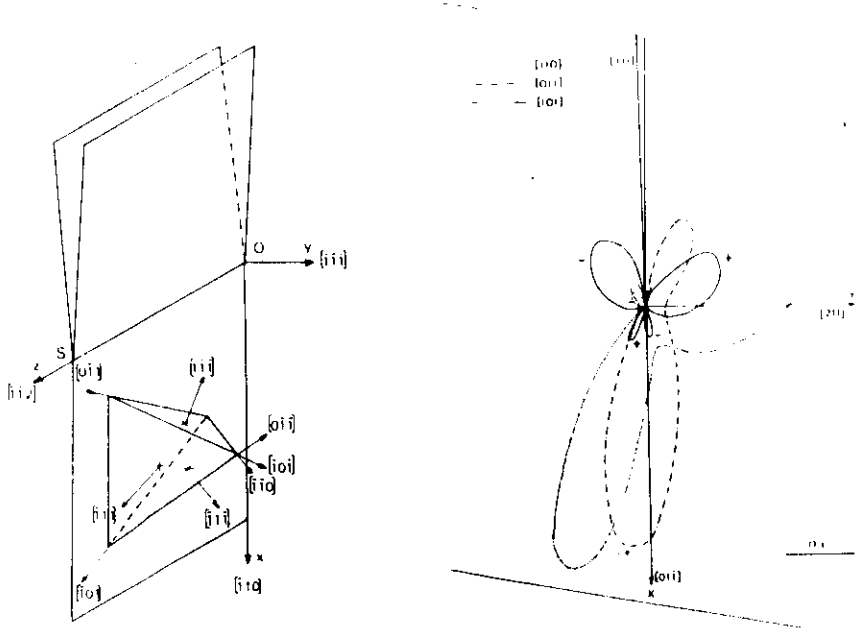

Figure 10 - a) Alpha orientation - Thomson tetrahedron orientation with respect to crack position
b) Constant resolved shear stress curve (CRSSC) for $(\bar{1}11)$ slip plane

III.2.2 - Beta orientation (figure 11)

As foreseen no dislocation are observed on $(\bar{1}\bar{1}\bar{1})$ plane. A more striking result is that only a few dislocations (less than ten) are observed in the plane which contains the crack tip. Thus nearly all the dislocations divide up into 80 % of dislocations with $\vec{b}$ parallel to the crack plane (slip systems $(\bar{1}\bar{1}1)[\bar{1}10]$ and $(\bar{1}1\bar{1})[\bar{1}01]$) and 20 % on slip systems $(\bar{1}\bar{1}1)[101]$ and $(\bar{1}1\bar{1})[\bar{1}\bar{1}0]$. Dislocations with Burgers vector a/2 $[0\bar{1}\bar{1}]$ belonging to both $(\bar{1}\bar{1}1)$ and $(\bar{1}1\bar{1})$ planes have not been unambiguously characterized.

III.2.3 - Gamma orientation (figure 12)

For this totally symetric orientation (figure 12b) no dislocation with Burgers vector either perpendicular to the crack plane or parallel to the crack propagation direction have been detected.

III.3 - Discussion

The problem to be solved is the determination of an criterion for dislocation generation at the crack tip. During single crystal homogeneous deformation, shearing takes place on the glide planes of maximum resolved shear stress (according to the so-called Schmid factor criterion). At crack tips although the situation is complicated by the high degree of triaxiality of the stress field which allows simultaneous activation of several glide systems, a stress criterion could apply.

However, a widespread opinion, relating stress relaxation to crack tip blunting, has been used for many years : the Burgers vector of the emitted dislocation is supposed to have a non zero component perpendicular to the crack plane (figure 13). This assumption is proved invalid by our experimental results (at least for alpha and beta orientations). Thus an other mechanism, called "shielding" has been introduced.

Afterwards, these three possible criteria will be rewieved.

III.3.1 - Stress field

The resolved shear stress τ acting on a dislocation line $\vec{\xi}$, with Burgers vector $\vec{b}$, gliding in plane $\vec{n}$ is given by :

$$\tau = (\bar{\bar{\sigma}}\,\vec{n})\,\vec{b}/b \qquad (5)$$

with a stress tensor derived from the elastic fracture mechanics :

$$\sigma_{ij} = \frac{K_I}{\sqrt{2\pi r}}\, g_{ij}(\varphi) \qquad (6)$$

It is convenient to express τ as a function of glide plane polar coordinates Φ and R (R is the distance between the considered point and the intersection point of the glide plane with the crack tip [2,19]) : $\tau = K_I\, H(\Phi)/\sqrt{2\pi R}$. Curves representing the locus of the points of the glide plane which experience a constant resolved shear stress can be drawn ; afterwards we shall refere to CRSS curves. The example displayed in figure 10 will be discussed in detail.

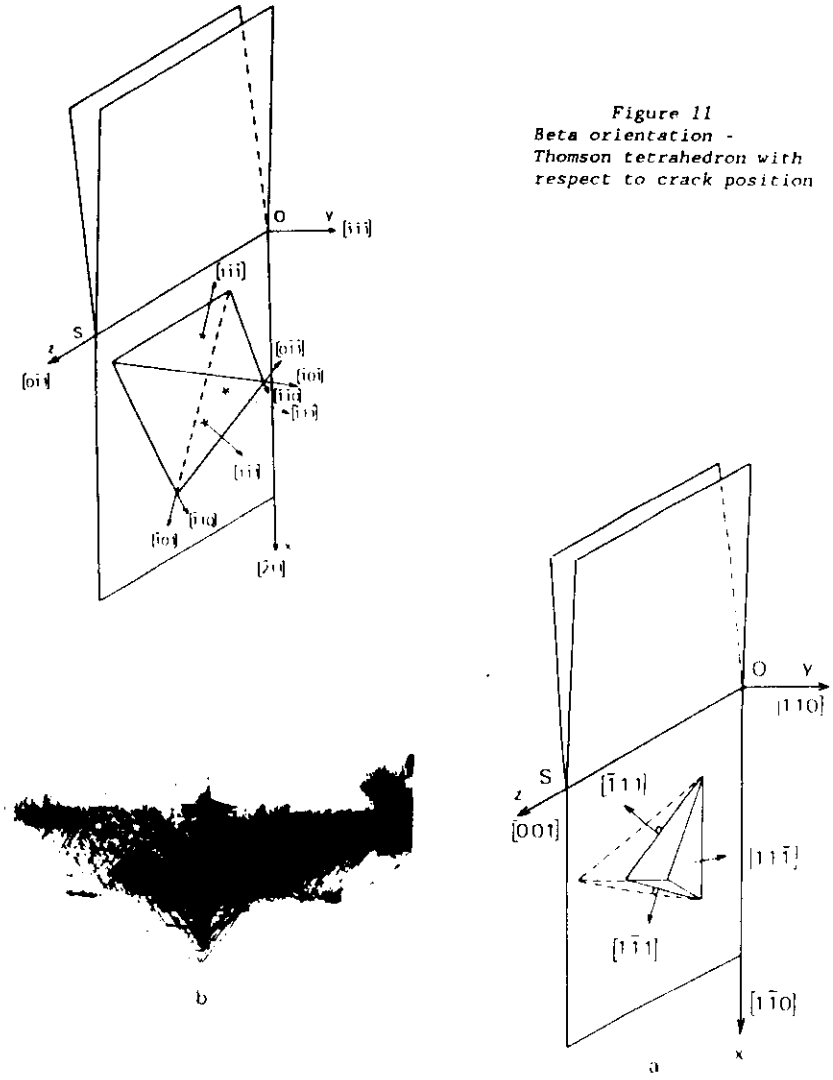

Figure 11
Beta orientation - Thomson tetrahedron with respect to crack position

Figure 12 - a) - Gamma orientation - Thomson Tetrahedron with respect to crack position - b) $\vec{g} = 1\bar{1}1$ topograph

The CRSS curves exibit either a single lobe (glide system $(\bar{1}11)\ [01\bar{1}]$, figure 10 : the + sign indicates that $H(\Phi)$ is positive, thus a dislocation $a/2[01\bar{1}]$ is repelled while a dislocation $a/2[0\bar{1}1]$ is attracted and disappears into the crack) or several small lobes (positive or negative, which can be seen in the $(\bar{1}11)[101]$ glide system). When development is restricted to some angular sector, development itself could be questionable. As a rule of thumb it appears that the most favoured system is the third one, i.e., $(\bar{1}11)[110]$, because of its greater extension. In fact, experimentally, only the first and the second systems really develop. That means that a stress criterion cannot totally account for our observations.

The same situation arises for the beta orientation [19] : the relative developments of observed glide systems contradict the calculated extensions as given by the CRSS curves. In particular the few dislocations gliding on the plane which contains the crack tip (figure 11) experience nearly the same stress as the majority of dislocations.

However the observed glide systems of the gamma orentation [18] obey the stress criterion. Thus in order to understand this discrepancy, a selection criterion based on interactions between different slip systems (annihilation, formation of junctions or Lomer Cottrell barriers) has been proposed [19] with some success, but this assumption has to be checked experimentally.

III.3.2 - Effect of dislocation emission on crack tip geometry

Returning to the alpha orientation (figure 10) it appears that development of a full loop of the $(\bar{1}11)[01\bar{1}]$ glide system leads to a jogging of the crack tip (figure 14) and the crack remains sharp. A different behaviour is expected from $(\bar{1}11)[101]$ glide system, for $\Phi < 0$ $(y < 0)$ a $a/2[\bar{1}0\bar{1}]$ loop develops and for $\Phi > 0$ $(y > 0)$ a $a/2[101]$ loop develops, leading to a localized blunting (figure 15). Some dislocation rearrangements, by cross-slip, could increase this blunting effect [45]. However it remains negligible compared to that obtained when the glide plane contains the crack tip (figure 13), like in the beta orientation. Because a few dislocations are then detected, we assume that blunting is not dominant in the relaxation mechanism.

III.3.3 - Shielding

Given a screw dislocation lying parallel to the crack tip of an unloaded crack. To remove the forces on the free surfaces of the crack, a force distribution has to be applied. In this case it is equivalent to introduce an image dislocation symetrical with respect to the crack tip [55-56] exerting a force on the dislocation :

$$f_i = - \mu b^2 / 4\pi r \qquad (7)$$

(μ is the shear modulus). From Newton's third law it appears that the crack must experience an equal and opposite force which can be related to a crack extension force G. In linear fracture mechanics this force is expressed as a function of a stress intensity factor ΔK :

$$G_{III} = \Delta K^2 / 2\mu \qquad (8)$$

(due to the screw character of the dislocation, antiplane shearing is assumed).

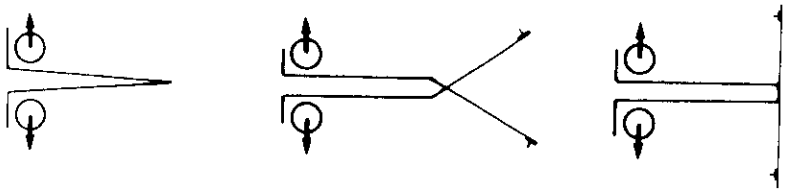

Figure 13 - During loading of a crack (a), edge dislocations develop on inclined planes (b) leading to crack blunting. When the Burgers vector is perpendicular to the crack plane, blunting is maximum (c)

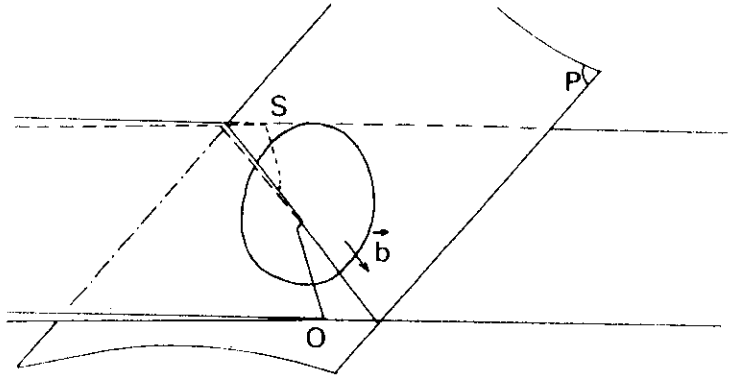

Figure 14 - Crack tip jogging by emission and development of a single dislocation on the glide plane P.

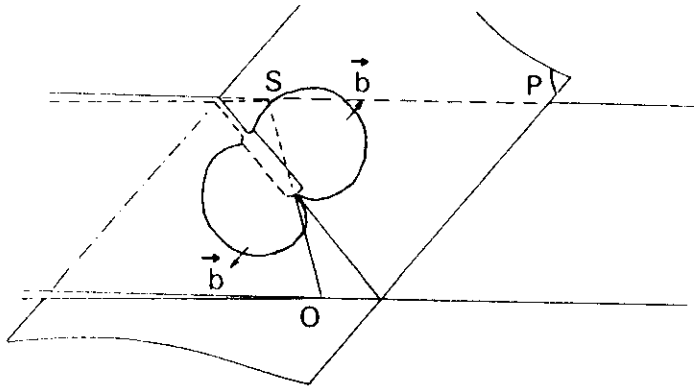

Figure 15 - Localized crack tip blunting by emission and development of two loops of opposite signs, on the same glide plane P.

If an external load, giving rise to a stress intensity K_{III} is superimposed, because stresses can be added, the resulting crack extension force becomes :

$$G_{III} = K_{III}^2/2\mu + \Delta K_{III}^2/2\mu + K_{III}\,\Delta K_{III}/\mu \qquad (9)$$

Depending on the sign of ΔK the dislocation can decrease or increase the crack extension force ; therefore when negative the dislocation has a shielding effect and when positive it has an antishielding effect [38].

This reasoning also holds for mode I as long as no blunting occurs otherwise the K concept fails. In the general mixed mode the shielding effect for dislocations parallel to the crack tip is related to the Burgers vector through a matrix relation :

$$[\Delta K] = \frac{\mu}{\sqrt{2\pi r}}\,[k]\,[b] \qquad (10)$$

whose k_{ij} components can be found in [57] and [58]

- Dislocation selection could be based on a shielding criterion, dislocations which lead to the highest shielding effect being the most likely to develop. This criterion differs from the usual minimum free enthalpy criterion because the crack extension force (i.e. the shielding) is related to the derivative of an energy ((3) of part A). It is not equivalent to a stress criterion because the latter is directly related to the applied elastic stress field while the former criterion only depends on the elastic energy of the loop, i.e. on its shape and Burgers vector.

This criterion is unfortunately difficult to handle because the matrix components k_{ij} have only been derived from the energy of straight dislocations parallel to the crack tip. That means that this treatment cannot account for dislocation nucleation, mechanism which is assumed to be a dominant parameter in brittle materials [55]. A 3D calculation is required. Exact calculation has been done for a half loop expanding on a glide plane containing the crack tip [59]. For general orientation only a rough estimate can be done [60].

However, eventhough no accurate estimates can be done, shielding relaxation at the crack tip must lead to a toughness increase which can be checked experimentally.

IV - TOUGHNESS INCREASE

IV.1 - Macroscopic approach

Full relaxation is assumed during high temperature loading under K_s when the effective stress intensity factor $K_e = K_s - |\Delta K(t)|$ drops under the thresold value K_{min} for dislocation emission :

$$K_{min} = K_s - |\Delta K_e| \qquad (11)$$

After relaxation the plastic zone is frozen in by cooling down. The sample is

then submitted to a tensile test. During crack opening the effective stress intensity factor is given by :

$$K_e = P\ f(a/w) - |\Delta K_o| \qquad (12)$$

where P is the load and f(a/w) the calibration function as introduced in part A. As long as the crack remains sharp, fracture will occur for $K_e = K_{IC}$ under the load P_c^* where :

$$K_{IC} = P_c^*\ f(a/w) - |\Delta K_o| = K_c^* - |\Delta K_o| \qquad (13)$$

Combining equation 11 and equation 13 we obtain :

$$K_c^* = K_{IC} - K_{min} + K_s \qquad (14)$$

Experimental results [61] as summarized figure 16 roughly agree with relation (14).

IV.2 - Results coherency

- In order to estimate the shielding effect we have [60] : i) roughly evaluated the shielding due to the individual dislocation (alpha orientation), taking into account its shape, Burgers vector and position ii) made the summation on the whole plastic zone using the dislocation distribution function as obtained by etch pit measurements iii) checked the resulting coherency with measured toughness increase.

- Our estimates show that ΔK_{II} and ΔK_{III} shieldings can develop. These parasitical effects, not expected from the mode I opening are related to departure of the loading symetry from crystallographic symetry. For instance, in alpha orientation, the crack propagation direction is a two fold symetry axis incompatible with the plane symetry required by pure mode I loading.

- Furthermore it appears that dislocations developing on either side of the crack plane ($[101](\bar{1}11)$ of figure 10) exhibit strong antishielding components, compared to dislocations which develop all around the crack tip ($[0\bar{1}1](111)$ of figure 10). This results could explain the higher proportion of dislocations of the second kind which were observed.

- For samples relaxed under 0.77 $MPa\sqrt{m}$ the shielding effect is estimated to - 1.2 $MPa\sqrt{m}$ [60], compared with the experimental results as obtained from relation 13, ranging from - 0.75 to - 0.50 $MPa\sqrt{m}$. Considering the roughness of the approximations the agreement is not too bad, we may conclude that shielding effects are important enough to account for the toughness increase following plastic relaxation.

V - EQUILIBRIUM PLASTIC ZONES

V.1 - Analytical solution

- This section deals with a theoretical study of dislocation distribution ahead of a crack tip. The problem has been solved using the K concept in order to avoid accounting for a specific geometry of the crack and the loading. For simplicity, mode III loading has been choosen. A semi-infinite crack is assumed. In this case a slip plane runs straight on from the crack plane (figure 17). Under loading ($K_{III} = K_s$) a set of straight parallel screw dislocations is emitted in the slip plane considered above. An equilibrium distribution is reached when the stress acting on every dislocation is equal to zero.

- When a continuous dislocation distribution $\rho(X)$ is assumed, an analytical solution can be derived from the following integral equation [62] :

$$\frac{K_s}{\sqrt{2\pi X}} - \frac{\mu b}{4\pi X} + \frac{\mu}{2\pi}\int_{A_1}^{A_2} \sqrt{\frac{Y}{X}}\ \frac{\rho(Y)\ dY}{X - Y} - \tau_y = 0 \qquad (15)$$

The first term corresponds to the external stress acting on a dislocation located at X from the crack tip (figure 17), the second to the image force [55-56-63], the third to the interaction with the other dislocations of the plastic zone. It must be pointed out that the usual interaction law between dislocations is modified by the vicinity of free surfaces, as shown by the conformal mapping method [63] or by the image dislocation distribution method [64]. The last term is the friction stress, a physical characteristic of the material. Because A_1, A_2 and $\rho(Y)$ are unknown, two extra relations are required. The first one is given by the total number of dislocations forming the plastic zone :

$$Nb = \int_{A_1}^{A_2} \rho(X)\ dX \qquad (16)$$

The second one will be derived from a condition on the effective stress intensity factor K_e when an equilibrium distribution is reached :

$$K_e = K_s - \frac{\mu}{\sqrt{2\pi}}\int_{A_1}^{A_2} \frac{\rho(Y)\ dY}{\sqrt{Y}} \qquad (17)$$

- When applying equation 15 to the first emitted dislocaiton it appears that a minimum value $K_o = \sqrt{2\mu b \tau_y}$ of K is required to overcome the image stress on this dislocation. It can be verified than an unstable dislocation position $A_o = \mu b/4\pi\tau_y$ corresponds to this value. With the introduction of dimensionless

parameters $k = \pi K/K_o$, $a = A/A_o$ and $p^2 = 1 - A_1/A_2$, equation 15 can be solved after some integral calculations [62] :

$$k_s = \underline{E(p)\ \sqrt{a_2}} + K(p)/\sqrt{a_1} \qquad (18)$$

$$k_e = \underline{K(p)\ \sqrt{a_1}} + E(p)/\sqrt{a_2} \qquad (19)$$

K(p) and E(p) correspond respectively to elliptical integrals of first and second kind. The variations of the plastic zone characteristics a_1, a_2 and N have been plotted in the (k_s, k_e) plane, respectively in figures 18 and 19.

V.2 - Discussion

- Chang and Ohr [65] have studied dislocation distribution ahead of the two tips of an embedded crack modelled by a continuous dislocation distribution. At the opposite of the so-called BCS model [66] they have allowed the existence of dislocation free zones (DFZ). It is valid to compare the limit case of long cracks for which no interaction occurs between the two plastic zones and our results. Chang and Ohr's model exactly matches the underlined terms of equations 18 and 19. Because the other terms are directly related to the image term - $\mu b/4\pi X$ of equation 15 we conclude that the image term is not properly taken into account when crack dislocation modelling techniques are used as pointed out in [68].

- No assumption has been done concerning K_e so far. Intuitively we could assume that full relaxation corresponds to $K_e = 0$. In Chang and Ohr's model this implies that the DFZ vanishes ; the solution than identifies with BCS solution. However from equation 19 of our calculation it appears that k_e must be strictly positive as soon as K_s overcome K_o. Hence, maximum but incomplete relaxation is achieved for the points of the (k_s, k_e) plane represented by the dotted line of figure 18 : in these conditions if any dislocation is added to the plastic zone, no equilibrium state can be found, one dislocation must reenter the crack.

- It can also be assumed that plastic zone growth is limited by the ability of the material to develop new dislocations. Dislocation activity stops when the effective stress intensity factor K_e drops under the threshold value K_I^{min} for source activation. The choice of either criteria depends on the brittle or ductile character of the material, i.e. the relative importance of K_{min} compared to K_o.

V.3 - Application to Silicon

Assuming $\tau_y = 6$ MPa it appears that $K_o = 0.018$ MPa$\sqrt{m}$ is much smaller than $K_{min} = 0.25$ MPa$\sqrt{m}$, hence the second criteria should apply. The shielding amount $|\Delta K_\infty|$ following maximum relaxation under K_s at high temperature can be experimentally obtained through equation 13. The effective stress intensity factor at the end of the relaxation process is given by $K_e = K_s - |\Delta K_\infty|$. The variations of K_e versus K_s are plotted figure 20. Experimental scattering is quite high but the average value is not too far from K_{min} value and much higher than K_o, confirming the choice of the second criterion.

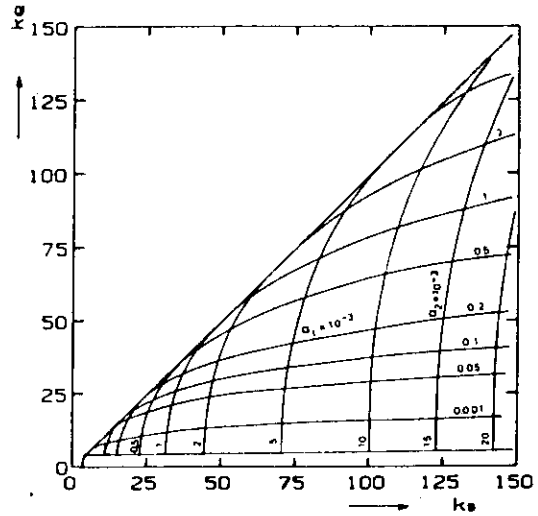

Figure 18 - Variations of the plastic zone size a_1, a_2 as a function of the applied stress intensity factor k_s and the effective stress intensity factor k_e

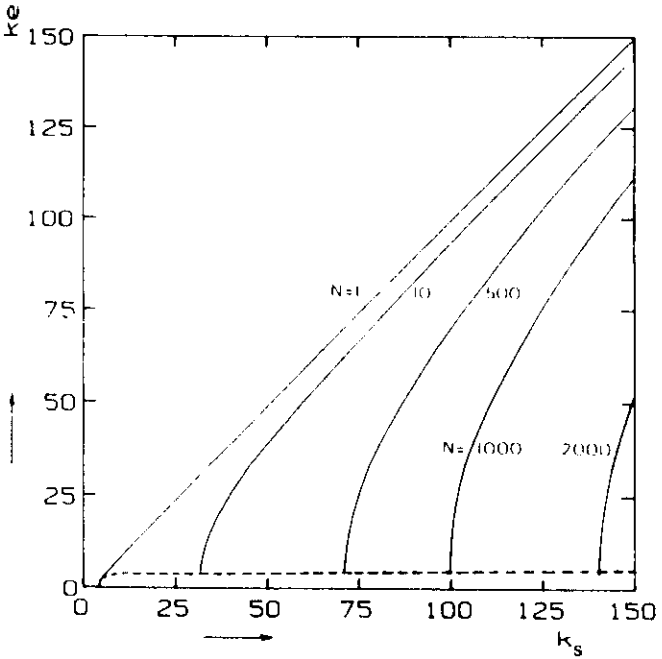

Figure 19 - Variations of the number N of dislocations as a function of k_s and k_e

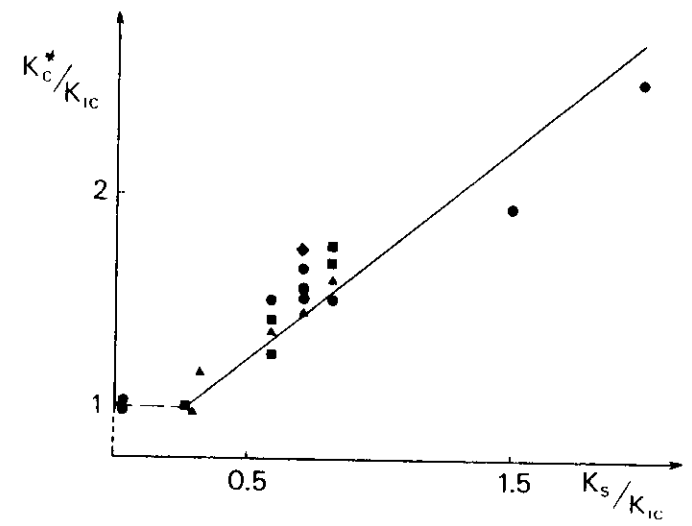

Figure 16 - Room temperature measured toughness K_c^* as a function of the high temperature relaxation load level K_s. The full line corresponds to relation 14.

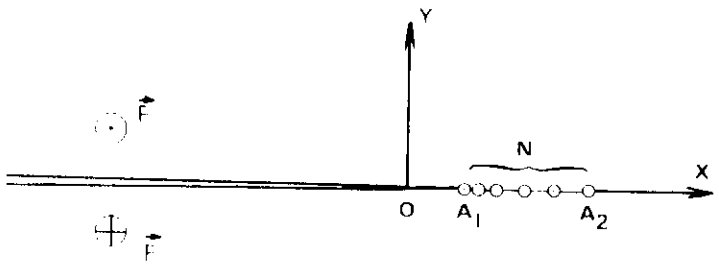

Figure 17 - Model of mode III plastic zone. N dislocations inside the $[A_1, A_2]$ space are in equilibrium under an applied K_{III} stress intensity factor

- Table 2 summarizes the experimental results obtained on five samples. From the corresponding K_e values the parameters of the plastic zone have been calculated (table 3).

Sample	K_I (MPa$\sqrt{m}$)	K_e	A_2 (nm)	N (by lobe)
F22	0.55	0.068	1.45	468
F14	0.66	0.186	1.45	796
F17	0.66	0.037	2.15	830
F36	0.77	0.168	2.75	2 900
F23	0.77	0.300	2.85	3 050

Table 2 - Experimental results

Sample	K_I	A_1	A_2	N
F22	0.55	1.74	3.29	866
F14	0.66	22.8	4.66	1 165
F17	0.66	0.22	4.76	1 264
F36	0.77	15.8	6.40	1 642
F23	0.77	75.5	6.23	1 455

Table 3 - Computed data

Despite the roughness of the approximations a satisfying agreement is obtained. Furthermore, improvements could be achieved by taking care of the confinment of the plastic zone by the non singular stress field in order to correct the overestimated value of A_2 ; likewise care should be taken of the orientation of slip planes with respect to the crack plane [67] for a true mode I loading.

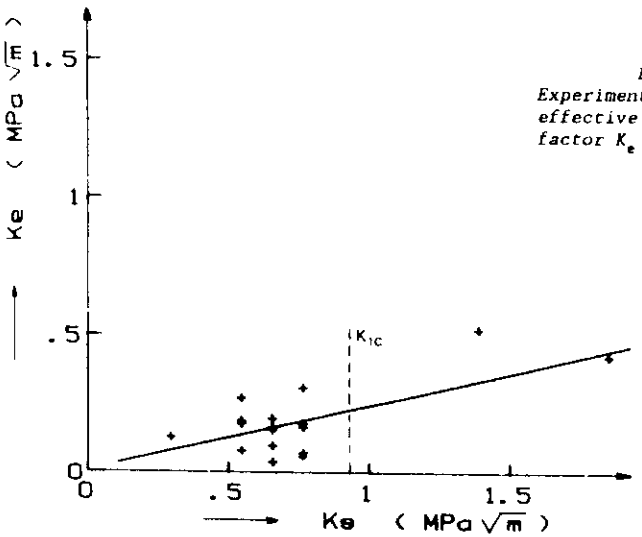

Figure 20
Experimental variations of the effective stress intensity factor K_e with the applied K_s

VI - BRITTLE TO DUCTILE TRANSITION

VI.1 - Transition temperature

Generally materials can exhibit different mechanical behaviours : the high brittleness of covalent crystals radically contrasts with the fully ductile behaviour of FCC metals. Depending on the ability of the material to emit dislocations from crack surfaces a brittle or ductile behaviour is expected [55, 69] : such a model, which seems to be accurate for the very brittle, or very ductile materials, fails when intermediate cases are considered (c.c. metals for instance). Furthermore we believe that the response of a material to a mechanical sollicitation, i.e. brittle failure or plastic yielding, does not depend only on the physical characteristics of the material, but also on some external parameters, such as loading rate. This point will be argued in the following.

During plastic relaxation the applied stress intensity factor K is, at least partially, counterbalanced by the crack shielding $-|\Delta K|$, leading to the effective stress intensity factor K_e :

$$K_e(t) = K(t) - |\Delta K(t)| \qquad (20)$$

Starting from a zero load under a constant loding rate $\dot{K}$ the corresponding variations with respect to time :

$$\dot{K}_e(t) = \dot{K}(t) - |\Delta \dot{K}(t)| \qquad (21)$$

must be strictly positive, at least until the threshold value for dislocation emission K_{min} is exceeded. The shielding rate $-|\Delta \dot{K}(t)|$ is thermally activated

through dislocation velocity. For low temperature, $\dot{K}(t)$ is the dominant term in equation 21, K_e is an increasing function of t, therefore brittle failure will occur for $K_e = K_{IC}$ (figure 21a). For high temperatures, $\dot{K}(t)$ can be counterbalanced or eventually overcome by the shielding term, this means that K_e goes through a maximum value (figure 21b). When smaller than K_{IC}, the crack opens in a fully ductile manner. A critical situation is achieved at temperature T_c for which the maximum value exactly equals K_{IC} (figure 21c). This temperature which limits two different behaviours of the material, quasi brittle for $T < T_c$ and fully ductile for $T > T_c$, is called brittle-to-ductile transition temperature (BDTT).

This transition mechanism is based on crack shielding [70,45] but the same reasoning applies when crack blunting is assumed [1,71,43]. In any case these models assume that BDT is not an intrinsic property of the material.

VI.2 - Modellization

Given a test temperature T_E, and a loading rate $\dot{K}$ low enough for dislocations to reach an equilibrium position for any K values. We assume that K_e is constant and equal to the threshold value for dislocation emission K_{min} : a steady state characterized by $\dot{K}_e = 0$ is achieved. Under these quasi-equilibrium conditions the decrease in the crack extension force due to N dislocations is equal to the force exerted by the crack on a superdislocation of Burgers vector Nb. The equilibrium condition is satisfied when this force is counterbalanced by the friction stress :

$$\frac{K^2}{2\mu} - \frac{K_e^2}{2\mu} = Nb\,\tau_y \qquad (22)$$

Derivation with respect to time leads to the nucleation rate :

$$\frac{\dot{K}\,K}{\mu b \tau_y} = \dot{N} \qquad (23)$$

If the tensile test is then performed under the same loading rate but at a lower temperature $T < T_E$, the decay in dislocation velocity forbids the establishement of an equilibrium situation. Thus shielding cannot be as complete as before, the effective stress intensity factor K_e must increase until a new steady state is restored. The temperature effect on dislocation velocity is conterbalanced by a stress level increase, characterized by a limit value K_e' (figure 22). The condition for constant velocity for simultaneous stresses and temperature variations is derived from the general relation :

$$v = v_o \left(\frac{\tau}{\tau_o}\right)^m \exp -\frac{Q}{kT} \qquad (24)$$

where v_o, τ_o, m and Q are constants :

$$\frac{dv}{v} - 0 = m\frac{d\tau}{\tau} + \frac{QdT}{kT^2} \qquad (25)$$

If the stress is supposed to be proportionnal to $K_e^{\ l}$ the later equation can be integrated, introducing the boundary condition $K_e^{\ l} = K_{min}$ for $T = T_\varepsilon$:

$$K_e^{\ l} = K_{min} \exp\left[\frac{Q}{mk}\left(\frac{1}{T} - \frac{1}{T_\varepsilon}\right)\right] \qquad (26)$$

According to this exponential variation with temperature of the $K_e^{\ l}$ plateau, we may reasonably assume that the initial slopes $\dot{K}_e(t=0)$ exhibit a strong temperature dependence also. Thus if the material fails at $T = T_c$ under a very high $\dot{K} = \dot{K}_c$" value, fracture at $T = T_c - \Delta T$ will occur under a much smaller $\dot{K}_c$' value (figure 22). That means that the brittle-to-ductile transition must be very sharp, as it has been checked experimentally (paragraph VI.3). T_ε is an approximate temperature above which the plastic zone is assumed to develop under quasi equilibrium conditions (any K increase is exactly counterbalanced by a shielding increase). Obviously T_ε must depend on the $\dot{K}$ choice. Introducing the fracture conditions, $K_e^{\ l} = K_{Ic}$ for $T = T_c$ in relation 26, this "equilibrium temperature" T_ε can be related to the BDTT (itself a function of $\dot{K}$)

$$K_{Ic} = K_{min} \exp\frac{Q}{mk}\left(\frac{1}{T_c} - \frac{1}{T_\varepsilon}\right) \qquad (27)$$

For $T_c = 993$ K, a physically acceptable $T_\varepsilon = 1062$ K value is obtained in Silicon (m = 1.2, Q = 2.2 ev).

The model assumes that dislocation movement is the limiting event and not the dislocation nucleation rate $\dot{N}$, mainly because the stress field decreases with distance to crack tip. The maximum rate, as given by equation 23 holds for the steady state at any temperature. During the non equilibrium transient regime this rate must increase from nearly zero to this maximum value. It results from our model assumptions that the higher the initial slope $\dot{K}_e(t=0)$, the lower the nucleation rate $\dot{N}$ and the temperature. That means that for temperatures close to T_c, but smaller than T_c, the number of emitted dislocations can be small, eventhough the applied K overcomes the K_{Ic} value (figure 22).

We cannot turn down the hypothesis that a K_e decrease arises after some plastic deformation due to a dislocation multiplication mechanism. If such a situation occurs after the steady state is achieved the K_e curve will exhibit a broad maximum. If not, no equilibrium configuration is involved and the previous calculations no longer hold.

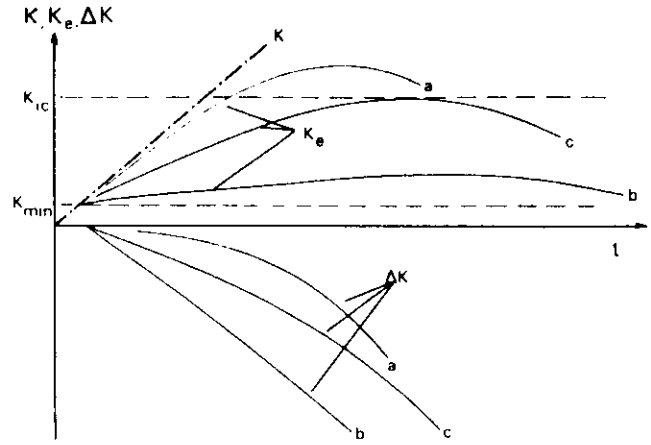

Figure 21 - Possible evolution of the effective stress intensity factor versus time, for different temperatures, $T < T_c$ curve a, $T > T_c$ curve b, $T = T_c$ curve c. The dashed line corresponds to the applied K variation.

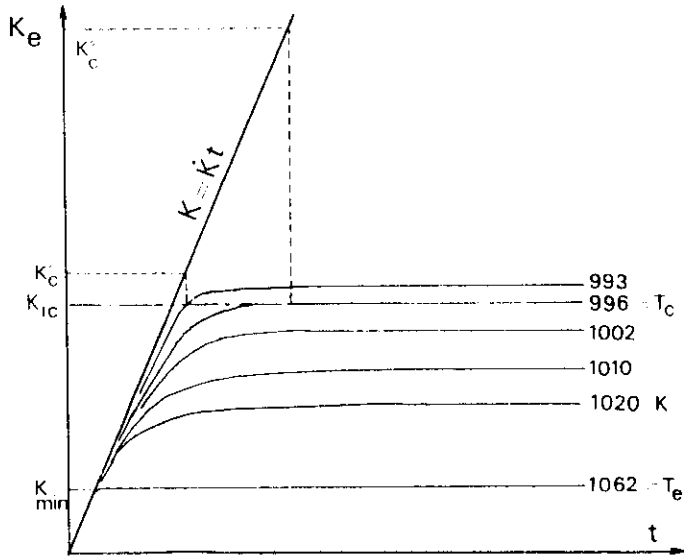

Figure 22 - Evolution of the effective stress intensity factor K_c as a function of temperature according to our model

VI.3 - Experimental results

Pre-cracked samples are opened at a constant rate $\dot{\delta}$, ranging from 1 μm/min to 500 μm/min. Below the BDTT the load-deflection curve is strictly linear. The material toughness K_c derived from the load at fracture P_c through the calibration curve is close to K_{IC} value (0.93 MPa$\sqrt{m}$) up to a few K below T_c.

The transition takes place in a very narrow range of temperature (2 K ≈). On the low temperature side of T_c, the load deflection curve remains linear up to fracture which occurs for a high stress intensity factor K_c (up to $3K_{IC}$). Above T_c the load deflection curve departs from linearity for $P > P_i$ (or $\dot{K} > \dot{K}_i$) and could exhibit a maximum when the test is continued. In this domain a general plastic yielding is observed leading to a macroscopic bending of the arms of the sample, avoiding ductile failure.

The temperature dependence of K_c/K_{IC} and K_i/K_{IC} for different deflection rates $\dot{\delta}$ of FZ and CZ silicon samples are represented figure 23 and 24 respectively. K_i values cannot be determined very accurately ; K_i is a decreasing function of the difference $(T-T_c)$ at a given $\dot{\delta}$. The T_c values measured on FZ Si are in close agreement to those obtained by St John for the same Silicon quality [1]. For a given deflection rate $\dot{\delta}$, the transition occurs at higher temperatures in CZ silicon, fer instance T_c is raised up to 41 K at $\dot{\delta}$ = 5 μm/min and 31 K at $\dot{\delta}$ = 50 μm/min.

VI.4 - Discussion

The BDTT, T_c, has been determined for several opening rates $\dot{\delta}$. Because of the linearity of the load deflection curve at this temperature a relation $\dot{K}(T_c)$ can be derived. The easiest way to compare plastic zone growth under different dynamic loading conditions is to deal with equilibrium configurations, i.e. with the full steady state characterized by $K_e = K_{min}$ and $T = T_\varepsilon$ ($\dot{K}$) (figure 22). These conditions correspond to a complete shielding ($\dot{K}_e = 0$) : as soon as the first dislocation is emitted, the shielding term $-|\Delta K(t)|$ exactly counterbalances the applied K. Because the shielding is thermally activated through dislocation mobility, one can write :

$$\dot{K} = |\Delta \dot{K}| = C^{ste} \times \exp - \frac{Q}{kT_\varepsilon}$$

or

$$\text{Log } \dot{K} = C^{ste} - \frac{Q}{kT_\varepsilon} \qquad (28)$$

But relation 27 shows that the replacing of T_ε by T_c in equation 28 only changes the value of the constant. Actually, such an exponential variation of $\dot{K}$ versus T_c has been observed (figure 25) : the activation energies thus derived correspond to 2.1 eV for FZ Silicon and 2.5 eV for CZ Silicon. The results agree fairly well with the value commonly reported in the literature for FZ crystals [52], 2.2. eV. For CZ crystals, the reported activation energy of 2.2 eV, for stresses higher than 4 MPa can increase markedly for lower stresses because of the dislocation pinning by oxygen atoms [72]. The coherency of our results can thus be achieved only if we assume that at T_ε, the plastic zone develops under a low stress level, probably around the friction stress τ_y [43].

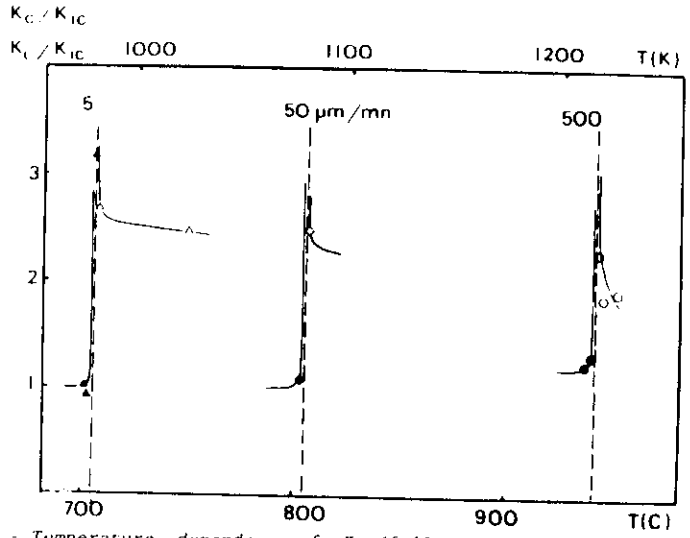

Figure 23 - Temperature dependence of K_c (full symbols) and K_i (open symbols) for different opening rates $\dot{\delta}$ (FZ Silicon)

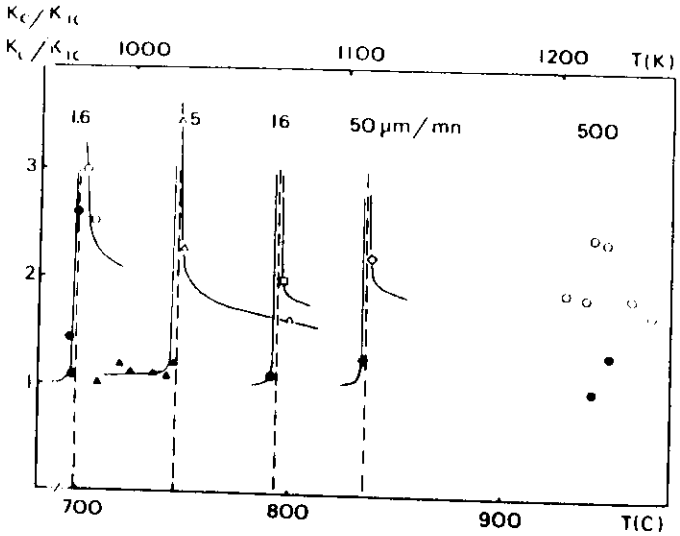

Figure 24 - Temperature dependence of K_c and K_i for different opening rates $\dot{\delta}$ (CZ Silicon)

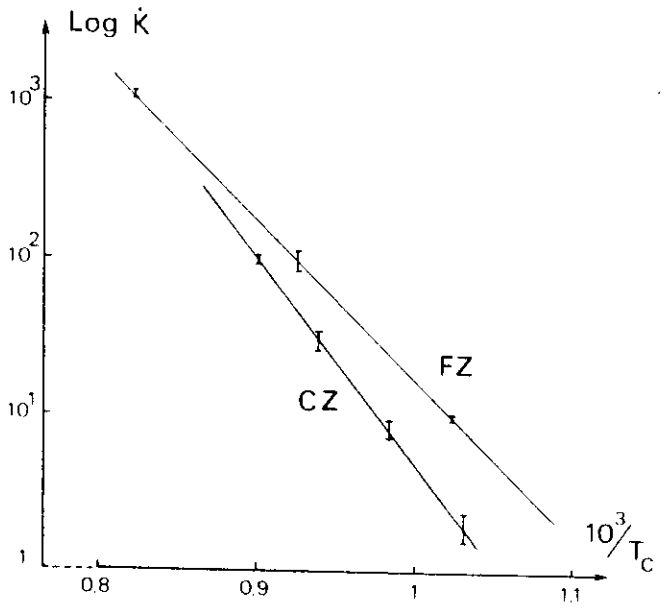

Figure 25 - Variation of the brittle to ductile transition temperature with the applied loading rate (K unit is the gf $mm^{-3/2}$ s^{-1}, equal to 310 $Pa/m^{3/2}$ s^{-1})

VI.5 - Dislocation sources

During cooling after crystal growth, a precipitation of interstitials combined with impurities occurs leading to a small defect population (some $10^6/cm^3$) which strongly depends on the pulling technique. Wether or not these defects can act as dislocation sources is not clear so far, especially because of their low density. Conversely, crack surface nucleation is suspected from T.E.M. observations eventhough this mechanism is not likely to occur according to theoretical estimations [55]. Thus dislocation origin is still an unanswered question.

VI.6 - Conclusions

The physical basis of the brittle to ductile transition have been presented. This transition is controlled by dislocation velocity. Eventhough this model gives a qualitative physical insight of this phenomenon, many points are still obscure and other experiments are needed. In particular, experiments under constant loading rates have to be perform in order to avoid intermediate parameters such as the crack opening and the sample compliance. Such tests are presently under way at L.U.R.E..

ACKNOWLEDGMENTS

I wish to thank Dr. A. GEORGE for hot and fruitful discussions, and the Staff of L.U.R.E, especially Dr. M. SAUVAGE, for provision of laboratory facilites.

SYMBOLS USED

- a - Crack length
- A_1, A_2 - Plastic zone limits - $a_1 = A_1/A_o$ with $A_o = \mu b/4\pi r_y$
- α, β, γ - Studied crystallographic orientations
- $\vec{b}$ - Burgers vector
- B - Sample thickness
- C - Sample compliance
- CRSSC - Constant resolved shear stress curve
- δ - Crack opening ($\dot{\delta}$ crack opening rate)
- ΔK - Crack shielding
- E - Young's Modulus
- φ, r - Polar coordinates related to the crack plane
- Φ, R - Polar coordinates related to a glide plane
- G - Crack extension force
- $\vec{g}$ - Diffraction vector
- γ - Fracture surface energy
- K - Stress intensity factor - $k = \pi K/K_o$ with $K_o = \sqrt{2\mu b \tau_y}$
- K_I - Stress intensity factor under mode 1 loading
- $K_{I\,min}$ - Threshold value of K_I for dislocation emission
- K_{IC} - Critical stress intensity factor for fracture
- K_e - Effective stress intensity factor
- K_s - Applied stress intensity factor for high temperature creep relaxation
- k_{ij} - Shielding matrix component
- μ - Shear modulus
- $\vec{n}$ - Direction perpendicular to a glide plan
- N - Number of dislocation in the plastic zone
- ν - Poisson ratio
- P - Applied load, P_c critical load for fracture, P_c^* critical load for fracture at 20°C of samples relaxed at high temperature
- $\vec{R}$ - Diffracted beam
- σ_{ij} - Stress tensor component
- T - Temperature
- T_c - Brittle to ductile transition temperature
- T_E - "Equilibrium" temperature for "stationnary" plastic zone growth
- τ_y - Friction stress
- τ_{eff} - Effective resolved shear stress
- τ_s - Applied resolved shear stress due to the singular term of the stress field expansion
- τ_i - Internal resolved shear stress due to plastic zone dislocations
- U - Stored elastic energy
- v - Dislocation mobility, depending on parameters m and Q
- w - Sample length

REFERENCES

[1] St John C.F., Phil. Mag., 1975, 32, 1193.
[2] Michot G., Badawi K., Abd El Halim A.R., George A., Phil. Mag., 1980, 42, 195.
[3] Michot G., Surface Science, 1987, 186, L561.
[4] Michot G., George A., Scripta Met., 1986, 20, 1495.
[5] Broek D., Elementary Engineering Fracture Mechanics (Martinus Nijhoff Publishers), 79.
[6] Srawley J.E., Gross B., NASA T.N.D-3820, 1967, 12.
[7] Griffith A.A., Phil. Trans. Roy. Soc. London, 1921, A221, 163.
[8] Irwin G.R., Wells A.A., Metall. Rev., 1965, 10, 223.
[9] Eshelby J.D., ISI Publications, 1968, 121, 13.
[10] Orowan E., Rep. Progr. Phys., 1949, 12, 48.
[11] Gilman J.J., Fracture, 1959, (Averbach & al. edits, MIT Press), 197.
[12] Michot G., George A., Scripta Met., 1988, 22, 1043.
[13] Messmer C., Bilello J.C., Jal. Appl. Phys., 1981, 52, 4623.
[14] Misra A., Finnie I., Jal Mat. Sci., 1979, 14, 2567.
[15] Puttick K.E., Hosseini M.M., Jal Phys. D., 1980, 13, 875.
[16] Chen C.P., Leipold M.H., Bull. Amer. Ceram. Soc., 1980, 59, 469.
[17] Bhaduri S.B., Wang F.F.Y., Jal of Mat. Sci., 1986, 21, 2489.
[18] Selatnia T., Thèse Docteur Ingénieur, INPL Nancy, France, 1986.
[19] Michot G., Thèse d'Etat, INPL Nancy, France, 1982.
[20] Grondwald K.D., Henzler M., Appl. Phys., 1984, A34, 253.
[21] Swain M.W., Lawn B.R., Burns S.J., Jal Mat. Sci., 1974, 9, 175.
[22] Gerberich W.W., Kurman E., Scripta Met., 1985, 19, 295.
[23] Jaccodine R.J., Jal Electrochemical Soc., 1963, 110, 524.
[24] Cahn J.W., Hanneman R.E., Surf. Sci., 1964, 1, 387.
[25] Sinclair J.E., Lawn B.R., Proc. Roy. Soc., 1972, A329, 83.
[26] Hsieh C., Thomson R., Jal Appl. Phys., 1973, 44, 2051.
[27] Lin I.H., Hirth J.P., Jal of Mat. Sci., 1982, 17, 447.
[28] Lewis M.H., Phil. Mag., 1966, 13, 1123.
[29] Wiederhorn S.M., Hockey B.J., Roberts D.E., Phil. Mag., 1973, 28, 783.
[30] Hockey B.J., Lawn B.R., Jal of Mat. Sci., 1975, 10, 1275.
[31] Appel F., Messerschmidt V., Kuna M., Phys. Stat. Sol., 1979, 55, 2, 529.
[32] Lawn B.R., Hockey B.J., Wiederhorn S.M., Jal of Mat. Sci., 1980, 15, 1207.
[33] Majumdar B.S., Burns S.J., Scripta Met., 1980, 14, 6, 653.
[34] Kobayashi S., Ohr S.M., Phil. Mag., 1980, 42, 6, 763.
[35] Ohr S.M., Narayan J., Phil. Mag., 1980, 41, 81.
[36] Kobayashi S., Ohr S.M., Scripta Met., 1981, 15 , 343.
[37] Kobayashi S., Ohr S.M., Jal of Mat. Sci., 1984, 19, 2273.
[38] Ohr S.M., Scripta Met., 1987, 21, 1681.
[39] Jacques A., George A., private communication.
[40] Westwood A.R.C., Goldheim D.L., Jal of Appl. Phys., 1963, 34, 11, 3335.
[41a] Chia K.Y., Burns S.J., Scripta Met., 1984, 18, 467.
[41b] Burns S.J., Scripta Met., 1986, 20, 1489.
[42] Behrensmeier R., Brede M., Haasen P., Scripta Met., 1987, 21, 1581.
[43] Brede M., Haasen P., Acta Met., 1988, 36, 8, 2003.
[44] Samuels J., Roberts S.G., Proc. Royal Phys. Soc., in press.
[45] Hirsch P.B., Roberts S.G., Samuels J., Proc. Royal Phys. Soc., in press.
[46] Burns S.J., Webb W.W., Trans. of Met. Soc. of AIME, 1966, 236, 1165.
[47] Burns S.J., Acta Met., 1970, 18, 969.
[48] Futagami K., Akashi Y., Jap. Jal of Appl. Phys., 1972, 11, 1265.
[49] George A., Michel J.P., Michot G., Nucl. Instr. Methods, 1983, 208, 731.
[50] Michot G., to be published.
[51] Michot G., George A., Scripta Met., 1982, 16, 519.
[52] George A., Champier G., Phys. Stat. Sol., 1979, 53, 529.
[53] Michot G., to be published

[54] Irwin G.R., Proc. 7th Sagamore Conf., 1960, IV-63.
[55] Rice J.R., Thomson R., Phil. Mag., 1974, 29, 73.
[56] Vitek V., Jal Mech. Phys. Solids, 1975, 24, 67.
[57] Kirchner H.O.K., Michot G., Mat. Sci. Eng., 1986, 79, 169.
[58] Lin I.H., Thomson R., Acta Met., 1986, 34, 187.
[59] Anderson P.M., Rice J.R., Jal Mech. Phys. Sol., in press.
[60] Michot G., to be published.
[61] Michot G., George A., Champier G., Proc. of the 4th European Conf. on Fracture, Leoben, Autriche, 1982, 30.
[62] Michot G., Fracture Control of Engineering Structures, ECF6, Amsterdam, 1986, 101.
[63] Majumdar B.S., Burns S.J., Acta Met., 1981, 29, 579.
[64] Li M.J.C., Dislocation Modelling of Physical Systems, Ashby and al. edits, 1980.
[65] Chang S.J., Ohr S.M., Jal Appl. Phys., 1981, 52, 12, 7174.
[66] Bilby B.A., Cottrell A.H., Swinden F.R.S. and K.H., Proc. Roy. Soc. London, 1963, A272, 304.
[67] Pande C.S., Masumura R.A., Chou Y.T, Acta Met., 1988, 1, 49.
[68] Louat N.P., Scripta Met., 1982, 16, 775.
[69] Anderson P.M., Rice J.R., Scripta Met., 1986, 20, 1467.
[70] Michot G., George A., Proc. ICSMA 7, Montreal, Pergamon Press, Oxford, 1985, 1187.
[71] Haasen P., "Atomistic of fracture", Nato Conf. Series, Series VI, Mat. Sci. Plenum Press, N.Y., 1983, 707.
[72] Imai M., Sumino K., Phil. Mag., 1983, A47, 599.